THE ASTROPHYSICAL JOURNAL, 440:200–209, 1995 February 10

NEAR-INFRARED [Fe II] AND Paβ IMAGING AND SPECTROSCOPY OF ARP 220

L. ARMUS, D. L. SHUPE, K. MATTHEWS, B. T. SOIFER, AND G. NEUGEBAUER
Palomar Observatory, California Institute of Technology, 320-47, Pasadena, CA 91125
Received 1994 July 13; accepted 1994 August 26

ABSTRACT

We have imaged the ultraluminous infrared galaxy Arp 220 in light of the near-infrared [Fe II] 1.257 μm and Paβ lines, and have obtained spectra in the *J*- and *H*-band atmospheric windows. Arp 220 is a strong source of [Fe II] and Paβ emission, with luminosities of 1.3×10^{41} and 9.2×10^{40} ergs s^{-1}, respectively. The [Fe II] and Paβ emission are both extended over the central 2″–3″, but with different morphologies. The Paβ line is strongly peaked at the position of the western nucleus seen at 2.2 μm (Graham et al. 1990) with a fainter "spur" in the direction of the eastern nucleus. The [Fe II] emission line shows a weak peak at the western nucleus along with diffuse emission extending to the east, but with no indication of a secondary maximum. The [Fe II] is more extended in the north-south direction than the Paβ line. Nearly 75% of the detected [Fe II] emission is spatially resolved. The overall [Fe II]-to-Paβ line flux ratio in Arp 220 is consistent with that seen over similar spatial scales in Seyfert 2 galaxies, yet larger than what is measured in galaxies with nuclear starbursts. The [Fe II]-to-Paβ line flux ratio is spatially variable being approximately 0.8 at the position of the western nucleus and approximately 2.0 at radii of up to 500 pc. We suggest that the extended [Fe II] emission is produced through the interaction of fast shocks with ambient gas in the ISM at the base of the outflowing, supernovae-driven superwind mapped by Heckman et al. (1987). The bolometric luminosity of the starburst required to power this wind is estimated to be at least 2×10^{11} $L_\odot$. If the spatially unresolved [Fe II] emission is produced via a large number of supernova remnants, the implied rate is ~ 0.6 yr^{-1}. The overall luminosity of such a starburst could account for a large fraction ($\frac{1}{2}$–$\frac{1}{3}$) of the Arp 220 energy budget, but the large deficit of ionizing photons (as counted by the Paβ luminosity) requires that the starburst be rapidly declining and/or have a low upper mass cutoff. Alternatively, dust may effectively compete with the gas for ionizing photons, or much of the ionizing radiation may escape through "holes" in the ISM. It is also possible that a buried AGN produces a large fraction of the unresolved [Fe II] and Paβ emission. We briefly discuss these possibilities in light of these new imaging and spectroscopic data.

Subject headings: galaxies: individual (Arp 220) — infrared: galaxies

1. INTRODUCTION

Arp 220 (UGC 9913) is the closest (72 Mpc for $H_0 = 75$ km s^{-1} Mpc^{-1}) and the best-studied member of the class of the ultraluminous infrared galaxies (ULIRGs) defined by Soifer et al. (1989) and Sanders et al. (1988). These galaxies all have $L_{IR} \geq 10^{12}$ $L_\odot$, comparable to the generally accepted minimum bolometric luminosities of quasars. Arp 220 has an $L_{IR} \sim 1.5 \times 10^{12}$ $L_\odot$. The facts that (1) all 10 ULIRGs in the *IRAS* Bright Galaxy Sample have distorted morphologies and/or multiple nuclei suggestive of a recent interaction and merger, (2) many of the ULIRGs have optical spectra indicative of sources of ionizing photons other than hot stars, and (3) the space density of these galaxies in the local universe ($z < 0.1$) exceeds that of quasars for $L > 10^{12}$ $L_\odot$ led Sanders et al. (1988) to suggest that these galaxies represent an intermediate stage in the evolution of a pair of merging spiral galaxies into an optically visible quasar. Arp 220 fits nicely into this model with its highly irregular optical morphology (Arp 1966), double nucleus (Graham et al. 1990a, hereafter G90), and LINER-like optical spectrum. It is often refered to as the "prototype" of the ULIRG class.

The strongest evidence for something other than hot stars contributing to the power in Arp 220 is its LINER-like optical spectrum, having strong low-ionization forbidden lines of [O I], [N II], and [S II]. There are other supporting data which also suggest this to be the case. DePoy, Becklin, & Geballe (1987) report the detection of a broad, FWHM ~ 3000 km s^{-1}, Bα line. However, the signal-to-noise ratio in the broad line wings in their spectrum was low, making an accurate measurement difficult. From an estimate of the free-free radio flux density at 2.7 mm, Scoville et al. (1991) argue that the ratio of the ionizing photon rate to the bolometric luminosity is smaller than what is typically found in starburst galaxies like M82 or NGC 253. Mazzarella et al. (1992) find two very red near-infrared nuclei in Arp 220, consistent with the presence of a pair of AGN behind a dust screen with $A_V = 7$–8 mag. If, however, the extinction to the nuclei is much larger, perhaps as large as $A_V = 50$–100 mag as implied by the silicate optical depth at 9.7 μm (Smith, Aitken, & Roche 1989), then Mazzarella et al. claim the Arp 220 nuclei contain nearly an order of magnitude more hot dust than is typically found in infrared luminous starburst galaxies, again suggesting the presence of a heavily obscured (pair of) AGN. Recent 18 cm VLBI observations of Arp 220 (Lonsdale, Smith, & Lonsdale 1993) suggest a very high brightness temperature ($T_b > 10^7$ K) core consistent with an active nucleus or a complex of extremely radio-luminous supernovae.

Although Arp 220 may harbor a buried AGN, there is evidence which suggests that a starburst may contribute significantly to the total energy budget. There is a very large reservoir of molecular gas, $\sim 2 \times 10^{10}$ $M_\odot$ (Scoville et al. 1991), strong PAH emission at 3.3 μm and strong CO absorption at 2.3 μm (Rieke et al. 1985). Starburst models with exponentially declining star formation rates and ages of 30–100 Myr have been

successfully fit to a wide variety of observations by Rieke et al. (1985) implying that a starburst could contribute up to 50% of the bolometric luminosity. Similarly, Mazzarella et al. (1992) show that the near-infrared colors at radii of 1″–2″ are the same in Arp 220 as seen in dusty starburst galaxies like M82 and NGC 253. Extended, diffuse emission at 15 GHz is taken by Sopp & Alexander (1991) as proof that a starburst is active in the circumnuclear environment of Arp 220. *Hubble Space Telescope* V, R, and I-band images (Shaya et al. 1994) contain a number of clumps within the inner kiloparsec which may be luminous stellar associations with luminosities greater than $10^9\ L_\odot$.

There thus exists evidence for both an AGN and a starburst in Arp 220—the question which has not been satisfactorily answered is how much each mechanism contributes to the overall energetics.

A crucial step in the evolution from ULIRG to optical quasar is the dissipation or removal of much of the obscuring matter not used in the early starburst phase from around the nascent black hole. It has been proposed that supernovae-driven superwinds may be responsible for this phase, and the presence of a large ($\sim$10 kpc), bipolar Hα + [N II] emitting bubble, along with split optical emission lines, indicates that this process is operating now in Arp 220 (Heckman, Armus, & Miley 1987, 1990). Superwinds drive fast ($\geq$100 km s^{-1}) shocks into the ambient ISM gas, producing optical line radiation and soft X-rays. Many of the ULIRGs, including Arp 220, have optical line flux ratios indicative of shock heating and split emission lines suggestive of outflow along a cone or bubble.

Low-ionization, near-infrared emission lines of [Fe II] at 1.257 and 1.644 μm are strong in regions of fast shocks, such as Galactic supernova remnants (Graham, Wright, & Longmore 1987, 1990). It has been suggested that both an increased gas phase abundance of Fe (from grain destruction) and ionization effects are responsible for the large enhancements (factors of 50 to 500) in the [Fe II]-to-H$^+$ ratios in supernova remnants as compared, for example, to those seen in Galactic H II regions. Recently, spatially resolved, spectroscopic studies of the nearby starburst galaxies M82 and NGC 253 (Greenhouse et al. 1991; Forbes & Ward 1993) show that strong [Fe II] emission is directly associated with young supernova remnants, and that spatial mapping of the [Fe II] emission may trace ongoing starbursts in dusty nuclei.

Arp 220 is a natural place to look for strong, extended near-infrared [Fe II] emission. To detect this emission, and map its spatial distribution in an attempt to discriminate between the various excitation mechanisms and compare the morphologies of the shocked and photoionized ISM, we have imaged Arp 220 in the light of redshifted [Fe II], Paβ, and the adjacent continuum using a set of narrow-band ($\sim$1%) filters. In § 2 we describe the observations and the data reduction. In § 3 we discuss the results in detail, and in § 4 we discuss the possible sources for the [Fe II] emission in Arp 220 and their importance for the overall energy budget.

2. OBSERVATIONS AND DATA REDUCTION

All observations reported here were made with the Palomar near-infrared camera mounted at the Cassegrain focus of the 200 inch (5 m) Hale telescope. The camera employs a 256 × 256 HgCdTe NICMOS3 array having a scale of 0.″167 pixel^{-1} at f/70, and an unvignetted field of view of 38″ × 36″. In addition, an offset guider maintains pointing accuracy to $\leq$0.″05 during long integrations. Images of Arp 220 were taken on 1994 February 24 UT under photometric conditions through narrow ($\Delta\lambda$ = 0.011–0.012 μm) filters centered at 1.268, 1.282, and 1.313 μm. At the redshift of Arp 220 (cz = 5450 km s^{-1}), the filters contain continuum at 1.245 μm, the [Fe II] 1.257 μm emission line, and the 1.282 μm Paβ emission line, respectively. Although the [Fe II] line is well centered in the 1.282 μm filter, the Paβ line is situated on the blue wing of the 1.313 μm filter and transmits only at the $\sim$75% level. All fluxes reported for this line have had this loss of efficiency taken into account. In lieu of taking images of blank sky, the telescope was moved by 15″–20″ between integrations, keeping the galaxy in the field of view at all times. Three 300 s exposures were taken in each of the 1.282 and 1.268 μm filters, while five 300 s exposures were taken through the 1.313 μm filter. For the remainder of this paper we will refer to rest wavelengths when discussing the imaging data.

The Arp 220 integrations were bracketed by observations of the photometric standards HD 129653 and HD 136754 (see Elias et al. 1982) and the offset guide star itself (while using a second guide star for position corrections). The latter ensured an accurate determination of the point spread function during the time of the Arp 220 integrations, which was measured to be in the range 0.″72–0.″75 FWHM. In addition to the narrow-band images, a set of four integrations was taken through each of two broadband J (1.12–1.37 μm) and K (2.00–2.40 μm) filters at the star of the Arp 220 sequence. The integration times for each of the J- and K-band images were 100 and 40 s, respectively.

The reduction of the imaging data consisted of sky subtraction, bad pixel interpolation, and flat-fielding for each frame, followed by registration and co-addition of the frames for each filter, and finally, flux calibration of the co-added data. The flat-fielding and sky subtraction were performed in a multistep process. First, a high signal-to-noise normalized flat-field frame was created from a series of twilight sky frames and divided into each galaxy and standard star frame. The initial sky subtraction was performed by differencing pairs of successive images. However, changes in the sky level from one image to the next left residual, spatially variable sky flux in the differenced frames. To correct for this residual background, a second set of flats was constructed by median filtering the unsubtracted guide star images and was divided into each frame. The residual sky then appeared as a constant offset in the portions of the images away from the galaxy and was easily subtracted.

For each filter, the images were averaged together after shifting to a common origin determined from the centroid of the nucleus. The field of view at the position of Arp 220 did not contain any foreground stars useful for accurate alignment of the average images created for each filter to a common center. However, since (1) the narrow-band filters are close in wavelength, (2) there is a single, strong nucleus obvious in each average filter image, and (3) the emission lines have equivalent widths which are small compared to the filter widths ($\sim$10–15%; see § 3), we have aligned the average frames on the bright, infrared nuclear peak. A scaled version of the 1.268 μm continuum image was then subtracted from each of the emission-line frames. An accurate scale factor was determined in each case by comparing the signals from the standard stars through the three filters.

In addition to the imaging observations, spectra in the J and H passbands at a resolution of $R \sim 100$ were taken on 1994

February 27 UT under nonphotometric conditions. A 0".8 wide slit was used, oriented in an E-W direction, and centered on the *J*-band continuum peak of Arp 220. This slit position was chosen to include both the western (brighter) and eastern infrared nuclei at the center of the Arp 220 system (see below). Five integrations of 400 s each and four integrations of 400 s each were taken covering the *J* and *H* bandpasses, respectively. In all cases the galaxy was moved approximately 10" along the slit between successive integrations and, as with the imaging, an offset guider was used to maintain pointing accuracy. The star BS 5727 (G0V), observed immediately following Arp 220, was used to remove the instrumental response and telluric absorption features from the galaxy spectra.

3. RESULTS

3.1. *Imaging: Paβ and* [Fe II] *Line Fluxes and Morphologies*

In Figure 1 we present our near-infrared *K*-band and continuum-subtracted Paβ emission-line images for direct comparison to the *R*-band and Hα + [N II] images of Armus, Heckman, & Miley (1990). The obscuring dust lane at a position angle of ~50° is evident in Figures 1*a* and 1*b*. We have used the astrometry of the infrared *K*-band data (G90) along with the positions of SAO stars in the optical frames, to correctly align the infrared and optical data. The small inserts in Figures 1*a* and 1*b* represent the full near-infrared frames presented in Figures 1*c* and 1*d*, with the central cross representing the position of the western nucleus. As has been pointed out by G90 the prominent *K*-band peak (the westernmost of the double near-infrared nuclei) sits behind the optical dust lane. Even at a resolution of ~0".75, the presence of the fainter, eastern nucleus is discernible in the *K*-band image as an elongation to the east of the primary nucleus. At Paβ we see an asymmetric nebula that extends over about 2", with a strong peak at the western infrared continuum nucleus. The total Paβ flux in our image (as measured through a 4".0 diameter circular synthetic aperture) is 1.1×10^{-14} ergs cm^{-2} s^{-1}, uncorrected for extinction, with ~50% arising from the unresolved western

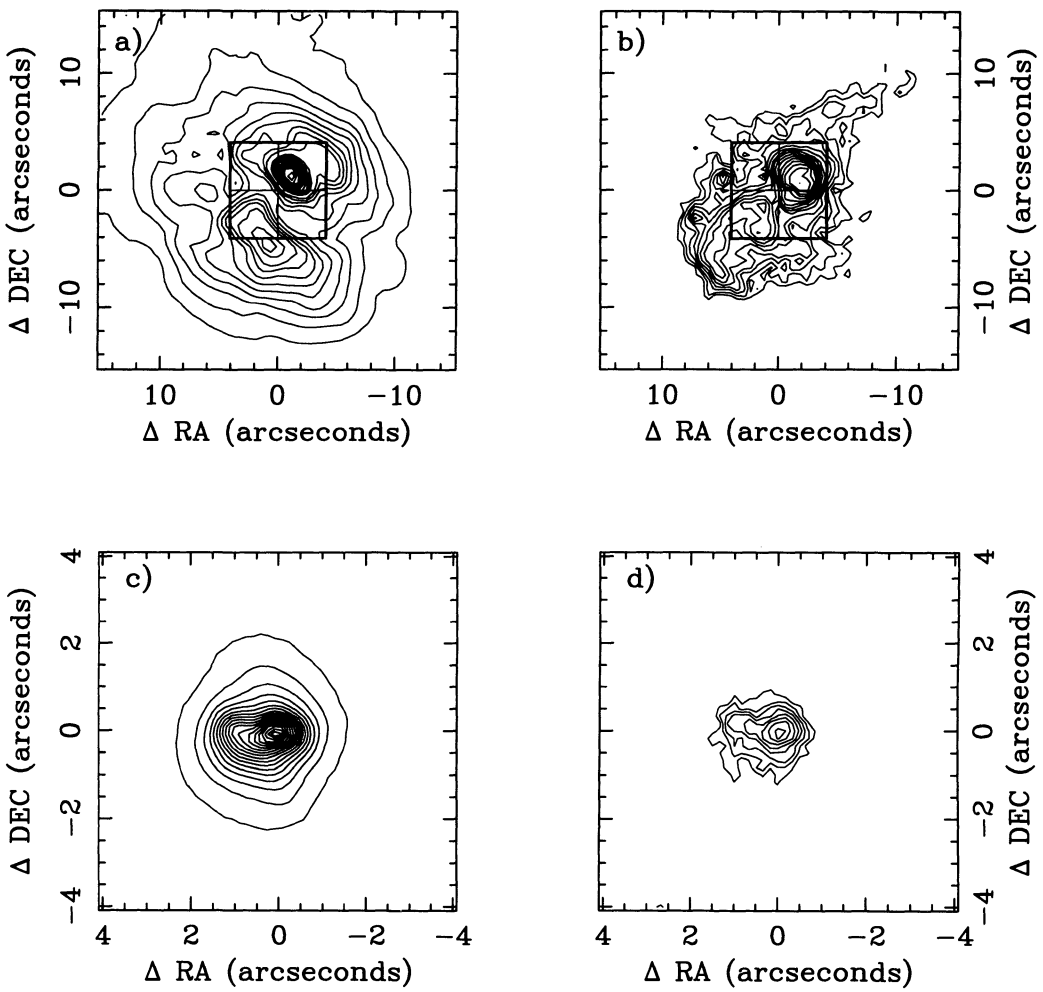

FIG. 1.—Optical and near-infrared images of Arp 220. (*a*) A broad *R*-band image progressing from 10% of the peak to maximum in steps of 5% of the peak. (*b*) A continuum-subtracted Hα + [N II] image with contours progressing from 20% of the peak to maximum in logarithmic steps, each a factor of 1.3 greater than the previous level. In both (*a*) and (*b*) the central box is the size of the infrared frames in (*c*) and (*d*), and the center of the cross represents the location of the western infrared nucleus (see text). The *K*-band and continuum-subtracted Paβ images are displayed in (*c*) and (*d*), respectively. The *K*-band image is contoured from ~7% of the peak to maximum in steps of 5% of the peak. The Paβ image is contoured from the 3 σ level in linear steps of 2 σ. Note the extent of the Paβ emission in (*d*) is ~2" and thus the strongest infrared line-emitting gas is located entirely behind the dust lane stretching across the optical images in (*a*) and (*b*).

nucleus. Although the Paβ nebula is predominantly east-west in extent, the spur to the east lies slightly north of the position of the infrared continuum nucleus identified in the 2.2 μm image of G90, which is separated by 0".95 from the western nucleus. The effect of the eastern nucleus on the inner K-band isophotes of Arp 220 can be seen in Figure 1*c*, although the nuclei are not clearly resolved in our image. Since the eastern nucleus is apparently obscured below ~ 2 μm, we do not expect to see it directly at Paβ. The emission we do see may be from ionized gas in the vicinity of the eastern nucleus visible just to the north of a sharply increasing column density of obscuring matter. The astrometric alignment of the K-band and optical data suggests that the western nucleus is on the northern edge of the dust lane in Arp 220. Southeast of this position the extinction increases rapidly toward the location of the eastern nucleus. Note that Mazzarella et al. (1992) measure an $H-K$ color for the eastern nucleus of $H-K = 1.4$–1.5 mag, approximately 0.1 mag redder than the western nucleus. In Figure 2*b* we show the continuum subtracted Paβ image from Figure 1*d*, but here smoothed with a Gaussian having a $\sigma = 1$ pixel kernel.

In Figure 2*c* we present the continuum-subtracted [Fe II] 1.257 μm image of Arp 220. Extended [Fe II] emission from Arp 220 is clearly detected over the central $\sim 2'' \times 3''$, with a peak at the position of the western infrared nucleus. The nebula is asymmetric, with extended emission toward the east in direction of the secondary nucleus. There is no strong peak at the location of the eastern nucleus, however. The [Fe II] morphology is clearer in Figure 2*d*, where we have smoothed the image in Figure 2*c* with a Gaussian having a $\sigma = 1$ pixel kernel. The peak at the position of the western nucleus is obvious, as is the extension to the east. The total [Fe II] 1.257 μm emission-line flux as measured through a 4".0 diameter circular synthetic aperture is 1.6×10^{-14} ergs cm^{-2} s^{-1}. Subtraction of a suitably scaled PSF from the [Fe II] image in Figure 2*c* suggests that nearly 75% of the total flux emission is spatially resolved. Due to uncertainties in the determination of the continuum subtraction scale factor (see below) and the absolute flux calibration we estimate our final [Fe II] and Paβ emission-line fluxes are accurate to $\pm 15\%$–20%.

Since the width of the filter used to measure the redshifted [Fe II] 1.2567 μm emission from Arp 220 is 0.011 μm FWHM,

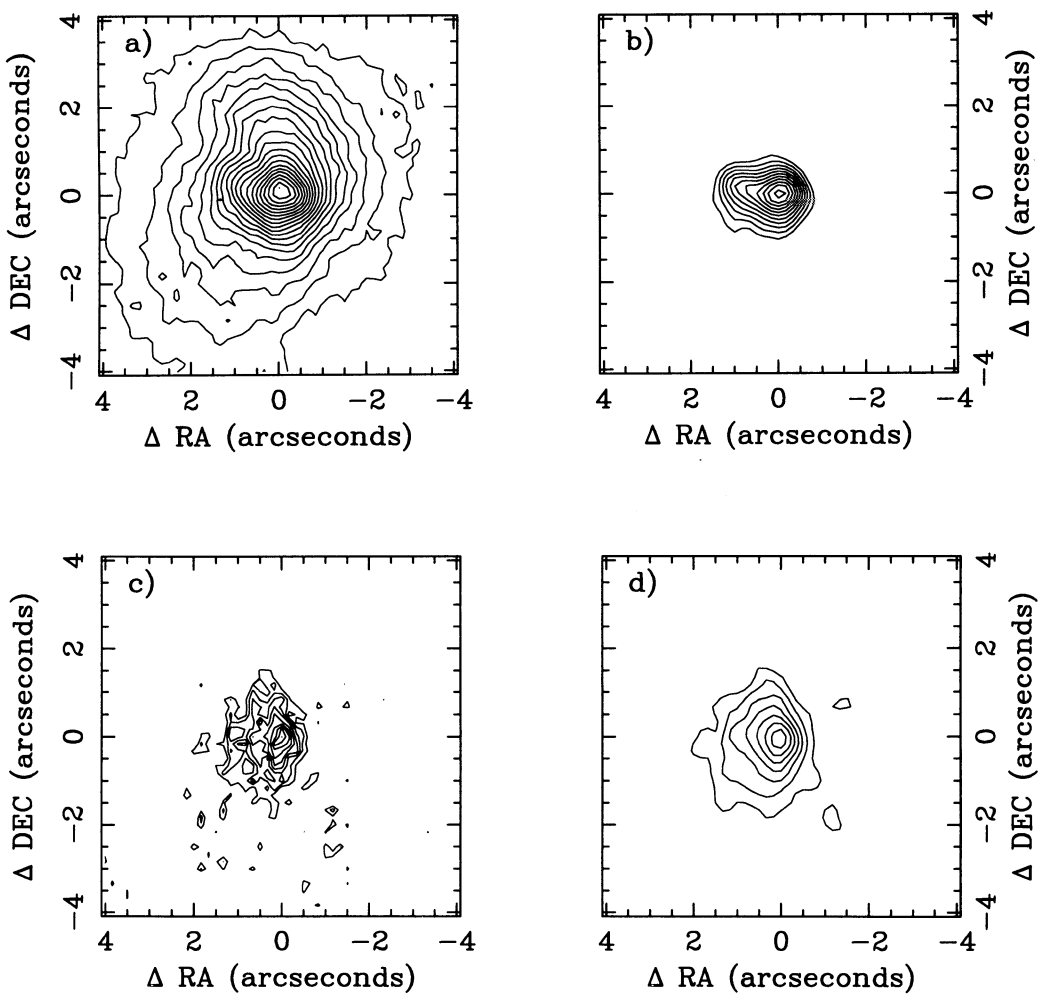

FIG. 2.—Comparison of the narrow-band near-infrared images of Arp 220. (*a*) The line-free 1.282 μm continuum. (*b*) The Paβ image reproduced from Fig. 1*d*, smoothed with a $\sigma = 1$ pixel Gaussian filter. (*c*) and (*d*) The [Fe II] 1.257 μm continuum subtracted frames, the latter being smoothed with a $\sigma = 1$ pixel Gaussian filter. The lowest contour in (*c*) is at the 3 σ level, with successive contours increasing linearly in 3 σ steps.

the He I line at 1.2528 μm can contribute to our calculated [Fe II] line flux. However, as we now show, this contribution is small, and we therefore neglect its effect. From Robbins (1968) we know that the He I 1.2528 μm/4471 Å emission-line flux ratio is 0.03 for $A_V = 0$ mag and $T = 10^4$ K. Under similar nebular conditions the He I 6678 Å/4471 Å flux ratio is 0.791 (Osterbrock 1989), implying a He I 1.2528 μm/6678 Å flux ratio of 0.038 for an $A_V = 0$ mag. The optical spectra of Armus, Heckman, & Miley (1989) imply an He I 6678 Å/Hα flux ratio of ≤ 0.01 over the inner 1″–3″ in Arp 220. For case B conditions, the intrinsic Hα/Paβ flux ratio is ~ 16.8; therefore, the He I 6678 Å/Paβ flux ratio in the nucleus is ≤ 0.19 for an $A_V = 0$ mag. This implies the He I 1.2528 μm/Paβ flux ratio ≤ 0.007 (independent of A_V) in the nucleus of Arp 220. If we measure the sum of the He I 1.2528 μm and [Fe II] 1.2567 μm line fluxes from our image (Fig. 2*c*) then the He I 1.2528 μm/[Fe II] 1.2567 μm line ratio $\leq 0.007 \times$ Paβ/(He I + [Fe II]). Since Paβ/(He I + [Fe II]) $\sim$ 1.0 to 2.0 over the central 2″–3″ in Arp 220 (see below), the contribution of the He I line to our [Fe II] flux is at most 1%–2%.

3.2. *Spectroscopy: J and H Band*

Near-infrared spectra covering the *J* and H atmospheric windows are presented for the central 2.″0 × 0.″8 of Arp 220 in Figure 3*a* and 3*b*. The ordinate is plotted in relative flux density units since the spectra were not taken under photometric conditions. The two prominent lines in the *J*-band spectrum are those of [Fe II] and Paβ at 1.257 and 1.282 μm, respectively, while the strong line in the *H*-band spectra is identified with the 1.644 μm line of [Fe II]. The equivalent widths of these lines are 0.0013, 0.0016, and 0.0019 μm, respectively. Uncertainties in the equivalent widths are typically 0.0002 μm. At the resolution of these spectra, approximately 3000 km s^{-1}, all three lines are unresolved.

The seeing conditions at the time of the spectral observations were similar to those at the time of the imaging observations. Since only the line equivalent widths were directly measurable from the spectra, we have used our calibrated 1.268 μm image to obtain a nuclear flux density applicable over the area of the extracted *J*-band spectrum. Line fluxes were subsequently derived from the spectra as a comparison to those derived from the narrow-band images. As a check on the flux calibration of the continuum data and the conditions at the time of the observations, we derived $J = 14.09$ mag over a 2.″5 diameter aperture, which compares favorably to the $J = 14.04 \pm 0.07$ mag measured in the same sized aperture by Carico et al. (1990). We have scaled the nuclear flux density in all subsequent calculations to match that seen by the latter authors in the 2.″5 diameter aperture. The [Fe II] 1.2567 μm line fluxes calculated from our narrow-band imaging data and the spectra agree well within the uncertainties, both measuring approximately 3.5×10^{-15} ergs cm^{-2} s^{-1} over the effective 2.″0 × 0.″8 slit. The Paβ flux measured from the continuum-subtracted image (through the projected slit aperture of 2.″0 × 0.″8) is, however, slightly larger than that measured from the *J*-band spectrum, being 5.3 versus 4.0×10^{-15} ergs cm^{-2} s^{-1}, respectively. Since the final Paβ image is strongly peaked on the continuum nucleus (more so than the [Fe II] image) we feel that a slight misalignment of the slit on the continuum nucleus can explain the difference between these values, and we adopt the image-derived value as more representative of the Paβ flux from the nucleus. Using a nuclear $J - H = 1.55$ mag (Mazzarella et al. 1992), we derive an [Fe II] 1.644 μm flux from the *H*-band spectrum of 7.5×10^{-15} ergs cm^{-2} s^{-1} over the effective 2.″0 × 0.″8 slit.

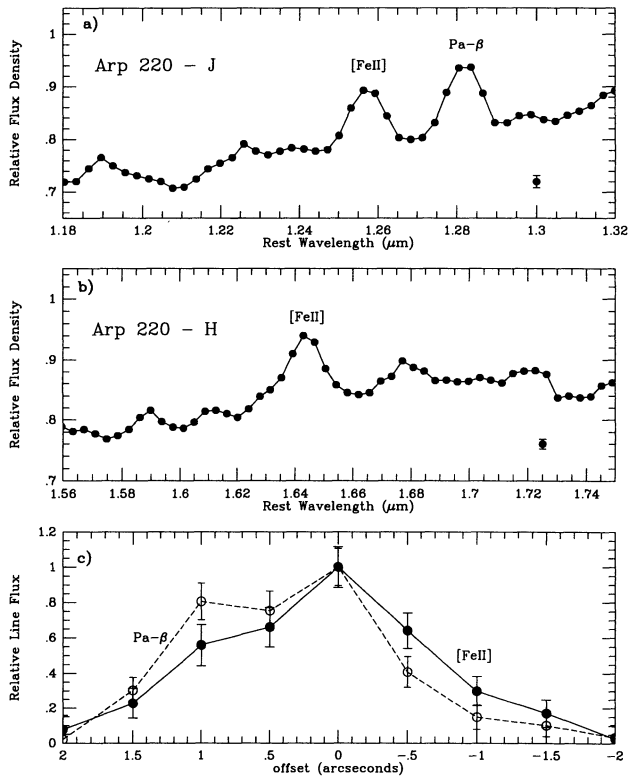

FIG. 3.—*J* (*a*) and *H*-band (*b*) spectra of the central 2.″0 × 0.″8 of Arp 220, extracted from an E-W oriented slit encompassing both eastern and western infrared nuclei. The spectral resolution is ~ 3000 km s^{-1}. The [Fe II] 1.257 μm and Paβ lines are prominent in the *J*-band spectrum, and the [Fe II] 1.644 μm line is strong in the *H*-band spectrum. Rest wavelength and relative flux density are plotted. The uncertainty in the flux density per resolution element is shown as a representative point in the lower right of each spectrum. (*c*) The [Fe II] 1.257 μm and Paβ lines as a function of position along the 0.″8 wide slit. Shown is a plot of the relative line flux (normalized to 1.0 at the position of the western infrared nucleus—defined as position 0.0 in these plots) measured in 0.″5 intervals over the central 4.″0. Note that the [Fe II] and Paβ lines have different spatial profiles, the former showing a sharper drop to the east and a shallower drop to the west than the latter. This is evident in the images of Fig. 2.

Given the strength of the Paβ line, and the resolution of the grism spectra, it is reasonable to consider the possible contamination of the [Fe II] 1.644 μm line by Br-12 at 1.641 μm. Based upon the strength of the Paβ line, and an intrinsic (case B) Br-12-to-Paβ flux ratio of 0.032 (Brocklehurst 1971) we estimate a Br-12 flux in the 2.″0 × 0.″8. aperture of 3.4×10^{-16} ergs cm^{-2} s^{-1}, for an $A_V = 10$ mag (see below). This is only 4.6% of the measured [Fe II] 1.644 line flux. Thus, although the [Fe II] and Br-12 lines are unresolved, the contamination of the measured [Fe II] 1.644 μm line by Br-12 is small, and within the measurement uncertainties, the effect of the Br-12 on the derivation of A_V (see below) is negligible.

In Figure 3*c* we present the profiles of the [Fe II] 1.257 μm and Paβ lines along the narrow slit. Each step represents a spectrum extracted in 0.″5 bins, with the zero offset position defined to be the western nucleus. The strengths of the lines have been normalized to unity at this location. The spatial distribution of flux in the [Fe II] and Paβ lines differ. The Paβ emission line falls more steeply than the [Fe II] line to the west, yet less steeply to the east, with a stronger contribution from

the eastern nucleus. This is entirely consistent with the imaging data of Figure 2. At the position of the western infrared nucleus the [Fe II]-to-Paβ line flux ratio is $\sim$0.8, while it appears to be slightly less ($\sim$0.6) at the position of the eastern infrared nucleus.

3.3. *Extinction*

We can use the J- and H-band spectral data as well as the Paβ imaging data to estimate the extinction to the near-infrared line-emitting gas in the vicinity of the Arp 220 nucleus. Since the 1.257 and 1.644 μm [Fe II] lines arise from the same upper level they provide a direct measure of the extinction. The spectral data indicate the 1.257 μm/1.644 μm line ratio $\sim$0.5, implying $A_V \sim 11.5$ mag averaged over the area covered by the slit. If we smooth the Paβ image to match the seeing in the Hα + [N II] image presented in Figure 1, and use an Hα/(Hα + [N II]) flux ratio of one-third for the central 2″ (Armus et al. 1989), we derive an Hα flux of 1.1×10^{-15} ergs cm^{-2} s^{-1} in a 2.″0 diameter aperture centered on the western infrared nucleus. The smoothed Paβ image has a flux of 7.6×10^{-15} ergs cm^{-2} s^{-1} in the same aperture, implying $A_V \sim 11$ mag, consistent with that determined from the [Fe II] spectral lines.

Although our data indicate $A_V = 10$–12 mag to the near-infrared line-emitting gas in Figures 1–2, much larger values of A_V can be derived by extrapolating measurements made at longer wavelengths. If we use the 9.7 μm silicate optical depth of $\tau \sim 7.0$ as measured in a 5.″6 diameter circular beam by Smith et al. (1989) along with the extinction curve of Rieke & Lebofsky (1985) we derive an $A_V \sim 90$ mag to the mid-infrared continuum-emitting region. Although the near-infrared photometry of Mazzarella et al. (1992) suggests the nuclear colors are consistent with an AGN behind $A_V \sim 7$–9 mag, the high-resolution K-band images of G90 clearly show that both nuclei (eastern and western) are individually resolved, and therefore the contribution of an AGN to the near-infrared light may be minimal. If the $J-H$ and $H-K$ colors of the nuclei are dominated by reddened starlight mixed with warm (600–1000 K) dust, the implied extinction is then much larger, possibly $A_V \sim 50$–100 mag.

Since we do not know the detailed distribution of the dust and gas in the nuclear region of Arp 220, we adopt an $A_V \sim 10$ mag as appropriate for the near-infrared line-emitting gas we have mapped. The total [Fe II] 1.257 μm line flux of 1.6×10^{-14} ergs cm^{-2} s^{-1} implies an extinction-corrected total luminosity of 1.3×10^{41} ergs s^{-1}, or about $33 \times 10^6 L_\odot$. Similarly, the total Paβ line flux of 1.1×10^{-14} ergs cm^{-2} s^{-1} implies an extinction-corrected total luminosity of 9.2×10^{40} ergs s^{-1}, and an ionizing photon rate of $\sim 1.3 \times 10^{54}$ s^{-1}, since $L(\mathrm{Pa}\beta) = 7.13 \times 10^{-14} N(\mathrm{H}^0)$ for a ionization bounded nebula where $N(\mathrm{H}^0)$ is the Lyman continuum photon rate (Osterbrock 1989). If $\sim$50% of the Paβ line flux is resolved (as suggested by PSF fits to our continuum-subtracted image), then $\sim 6 \times 10^{53}$ ionizing photons s^{-1} are required to ionize either the extended or the spatially unresolved emission-line gas.

4. DISCUSSION

The major result presented in this paper is that Arp 220 is a strong source of [Fe II] and Paβ emission, with both J-band lines being spatially extended over the central 2″–3″ ($\sim$1 kpc). Although the near-infrared line emission sits entirely behind the dust lane bisecting the nucleus, the [Fe II] and Paβ line morphologies are different, indicating a spatially variable [Fe II]-to-H$^+$ line flux ratio. The extinction to the near-infrared line-emitting regions in the central 2″–3″ is likely close to $A_V \sim 10$–12. We address here the possibility of determining the source of the [Fe II] emission, and explore using the strength of the [Fe II] to estimate the star formation rate and thus the fraction of the bolometric luminosity contributed by a starburst.

4.1. *Comparison with Other Galaxies*

Near-infrared studies have reported large values of the [Fe II]-to-H$^+$ emission-line ratios for starburst and active, mostly type 2 Seyfert, galaxies. Ionization as well as abundance effects (enhancements in the gas-phase Fe abundance due to grain destruction) have been used to explain line ratios which can be factors of 50–500 greater than those seen in H II regions (Graham et al. 1990b; Greenhouse et al. 1991; Mouri, Kawara, & Taniguchi 1993).

Goodrich, Vailleux, & Hill (1994) have recently measured the [Fe II] 1.257 μm and Paβ lines through narrow (1.″5–3.″0 wide) slits in a sample of 15 Seyfert 2 nuclei. The average [Fe II]-to-Paβ flux ratio among the 15 Seyfert 2 nuclei is 1.3, with values ranging from $\sim$0.3–4.4. In nearly all of the Seyfert 2 galaxies measured by Goodrich et al. the width of the [Fe II] 1.257 μm line is similar to that of the narrow component of the Paβ line, typically 300–600 km s^{-1}, suggesting that the [Fe II] emission is predominantly generated in the narrow line region (NLR) surrounding the nucleus. Other studies (often comparing the [Fe II] 1.644 μm line to the optical [O III] 5007 Å and/or Hα lines) have come to the same conclusion (Rieke & Lebofsky 1981; Moorwood & Oliva 1988; Kawara, Nishida, & Taniguchi 1988; Oliva & Moorwood 1990). Recent [Fe II] 1.644 μm line imaging of NGC 1068 by Blietz et al. (1994) suggests that the [Fe II]-emitting zone is spatially coincident with the NLR.

A great deal of the work in this area has traditionally focused on the [Fe II] 1.644 μm/Bγ ratio. The conversion from our measured [Fe II] 1.2567 μm/Paβ ratio in Arp 220 to an [Fe II] 1.644 μm/Bγ ratio requires knowledge of the extinction to the infrared line emitting region. If we adopt an $A_V = 10$ mag, then ([Fe II] 1.644 μm/Bγ) $\sim 2.6 \times$ ([Fe II] 1.257 μm/Pβ). For an $A_V = 0$ mag, the conversion factor is 4.5 (Nussbaumer & Storey 1988; Savage & Mathis 1979).

There are, at the time of this writing, 10 starburst galaxies with measured [Fe II] 1.644 μm-to-Bγ line flux ratios reported in the literature (Moorwood & Oliva 1988; Kawara et al. 1988; Lester et al. 1990). Most of the observations have been made through apertures which project to physical scales ranging from 100 pc to 2 kpc. The average measured [Fe II] 1.644 μm-to-Bγ line flux ratio for the starburst galaxies as a class is 1.4, with the ratio extending from 0.6 to 2.9, implying [Fe II] 1.257 μm-to-Paβ flux ratios of about 0.2–1.0.

Over the central 3″ (about 1 kpc) in Arp 220, the [Fe II] 1.257 μm-to-Paβ flux ratio is $\sim$1.4, comparable to that found for the Seyfert 2 galaxies. However, the [Fe II]-to-Paβ flux ratio has a strong spatial dependence. At the positions of the two nuclei the ratio is $\sim$0.8 for the unresolved line-emitting gas, while the extended off-nuclear gas has a ratio of $\sim$2.0. For an $A_V = 10$ mag, the [Fe II]-to-Paβ flux ratios in Arp 220 imply [Fe II] 1.644 μm-to-Bγ flux ratios of approximately 2 and 5, respectively. The nuclear (spatially unresolved) [Fe II] 1.257 μm-to-Paβ line flux ratio in Arp 220, therefore, is comparable to that seen in the Seyferts of Goodrich et al. (1994) and also to some of the starburst galaxies with the largest measured [Fe II]-to-Bγ ratios. However, the extended [Fe II] emission

has an implied [Fe II]-to-Bγ ratio larger than that seen in any starburst galaxy. Although this suggests that the extended emission may not be from a starburst directly, it should be noted that individual Galactic supernova remnants can have [Fe II] 1.257 μm-to-Paβ line flux ratios of ~3–15, depending upon the physical conditions in the vicinity of the shocked filaments (Oliva, Moorwood, & Danziger 1989; Graham et al. 1990b).

The only other luminous infrared galaxy to be mapped in [Fe II] is NGC 6240, which is very similar to Arp 220 in many respects, but which has a bolometric luminosity a factor of about 2 less. Both are dusty, merging, double-nucleus systems, with evidence for large-scale shocks operating in and around their nuclei. NGC 6240 has the largest [Fe II] 1.655 μm-to-Bγ line flux ratio measured for any galaxy, ~17 in a 1.7 kpc diameter circular aperture (Lester, Harvey, & Carr 1988). Through near-infrared Fabry-Perot mapping of NGC 6240, van der Werf et al. (1993) find that the [Fe II] emission is concentrated at the positions of the merging nuclei, with only 10%–20% of the total [Fe II] 1.644 μm emission being spatially extended, unlike Arp 220 where most of the [Fe II] emission is extended over $\frac{1}{3}$–1 kpc scales. Van der Werf et al. suggest that the [Fe II] emission in NGC 6240 is generated by starburst activity in the merging nuclei. Adopting an extinction of $A_V = 4$ mag (Rieke et al. 1985) and a distance of $D = 97$ Mpc for NGC 6240, the total [Fe II] 1.644 μm luminosity is 2×10^{41} ergs s^{-1}, implying an intrinsic [Fe II] 1.257 μm line luminosity of 2.7×10^{41} ergs s^{-1}, or about a factor of 2.2 larger than we have measured for Arp 220 (see below).

We can summarize the [Fe II] emission and [Fe II]-to-H$^+$ line flux ratios in Arp 220 in comparison to other studied galaxies as follows. The global (averaged over the central kpc) [Fe II]-to-Paβ line flux ratio in Arp 220 is comparable to that seen over similar spatial scales in Seyfert 2 galaxies, but larger than that seen in nuclear starburst galaxies. At face value it appears that the [Fe II] emission in Arp 220 (by virtue of the [Fe II]-to-H$^+$ line ratios) could be excited by a buried AGN similar to those believed to exist in the nuclei of Seyfert 2 galaxies. However, there are two reasons why we feel a buried AGN is not responsible for the extended [Fe II] emission in Arp 220. The [Fe II] and the Paβ are clearly extended, yet the [Fe II] and Paβ emission-line morphologies are different. Approximately 75% of the [Fe II] emission is emitted on scales of greater than 1″, or 350 pc. Since this is large compared to the canonical size of the NLR surrounding a Seyfert nucleus, and it is the NLR which is likely to be responsible for most of the [Fe II] emission in Seyfert galaxies, the physical distribution of the [Fe II]-emitting gas in Arp 220 suggests that a central active nucleus is not responsible for the strong, extended [Fe II] emission. Although the extended narrow line region (ENLR) seen in some Seyfert galaxies can be 1 to a few kpc in size (see Perez-Fournon & Wilson 1990), the different Paβ and [Fe II] morphologies suggest that a single excitation mechanism is not responsible for the bulk of the flux measured in both emission lines in Arp 220.

Blietz et al. (1994) have recently mapped the nearest Seyfert 2 galaxy, NGC 1068, in the [Fe II] 1.644 μm line. Although the [Fe II] emission is extended on scales of 8″ × 4″ (radii of up to ~250 pc), the emission follows the spatial distribution of the ionized gas in the NLR (Evans et al. 1991). Blietz et al. suggest the [Fe II] emission in this Seyfert galaxy is excited either by nuclear X-ray radiation in the NLR, or by the interaction of a nuclear jet (see the 5 GHz map of Wilson & Ulvestad 1983) with ambient molecular clouds around the nucleus. Since the [Fe II] emission in Arp 220 has a different morphology than the Paβ emission, which should trace the NLR if a buried AGN is energetically important, it is unlikely that the scenario which has been suggested for NGC 1068 applies here. Furthermore there is no radio jet in Arp 220 which follows the collimated emission from a buried AGN as there is in NGC 1068.

Since Arp 220 is known to have a large-scale, outflowing superwind (Heckman et al. 1987, 1990), and it is suspected of being host to a starburst which may be of considerable power (Rieke et al. 1985; Mazzarella et al. 1992), we suggest that the extended [Fe II] emission is produced as a result of fast ($V > 100$ km s^{-1}) shocks at the base of the outflowing superwind. Although the position angle of the diffuse [Fe II] emission in Arp 220 is different from that determined for the large-scale outflow, the infrared imaging data only map the highest surface brightness regions in the central 2″–3″, which mostly sits behind the thick dust lane seen in Figure 1. The dust lane, which is nearly, but not exactly, perpendicular to the large-scale Hα + [N II] nebula, is likely to be the collimating agent as the shocked gas is expelled from the inner kiloparsec. In the superwind phenomenon, large, optical-line, and X-ray–emitting nebulae are often seen on scales much larger than the starburst which is the ultimate source of their power. Since shocks are a ubiquitous feature of the winds, strong [Fe II] emission is expected over an extended region.

4.2. *Energetics of the Starburst*

If the extended [Fe II] emission in Arp 220 is produced in a starburst through the action of a large number of supernova remnants, we can use the [Fe II] luminosity to estimate the supernova rate, and, by comparison with starburst models, calculate the contribution a burst to the bolometric luminosity of the galaxy.

The spatially resolved [Fe II] 1.257 μm luminosity in Arp 220 is $\sim 9 \times 10^{40}$ ergs s^{-1} (for an $A_V = 10$ mag), implying an [Fe II] 1.644 μm line luminosity of $\sim 7 \times 10^{40}$ ergs s^{-1} (Nussbaumer & Storey 1988). We can use the [Fe II] luminosity to place an upper limit on the strength of a circumnuclear starburst in Arp 220 by assuming that all the extended [Fe II] emission is produced directly by supernovae remnants associated with the burst. The total [Fe II] emission (in the 1.644 μm line for example) can then be parameterized as $L \sim \mathrm{SNR} \times (\langle t \rangle) \times (\langle L \rangle)$, where SNR is the supernova rate, $\langle t \rangle$ is the [Fe II]-emitting lifetime of a single remnant, and $\langle L \rangle$ is the average [Fe II] luminosity of an individual supernova remnant. Although complete [Fe II] maps of Galactic supernova remnants are very difficult to obtain due to their large projected sizes and patchy extinction, as well as the fact that the [Fe II] life-time estimates are somewhat model dependent, values of 10^3 $L_\odot$ (3.9×10^{36} ergs s^{-1}) in the 1.644 μm line and 10^4 yr are often taken as representative of the most luminous remnants in our Galaxy (Oliva et al. 1989). If the extended [Fe II] emission in Arp 220 is produced by SNRs associated with a circumnuclear starburst, the implied supernova rate is then SNR ~ 1.8 yr^{-1}. An ongoing (continuous star formation) burst with a supernova rate of this magnitude could easily account for the entire energetic output of Arp 220 (see models by Leitherer & Heckman 1995).

If the extended [Fe II] emission is produced directly from a collection of supernova remnants, then we would expect extended nonthermal radio emission from the supernovae and supernova remnants on the same physical scales. At 15 GHz,

Sopp & Alexander (1991) measure an extended source on scales of about one arcsecond with the VLA. The same authors fail to detect extended 6 cm emission, and their 0".4 beam measurement (211 mJy) is consistent with the small and large array spacing VLA data presented by Norris (1988) and Condon (1980). Sopp & Alexander assert that the extended radio emission has a thermal spectrum, and is produced in a circumnuclear starburst in Arp 220. However the scale of this proposed starburst (between ~0".5 and 1".0 in radius) is much smaller than the size of the [Fe II]-emitting zone we have mapped here.

An alternative explanation for the extended [Fe II] flux (besides a collection of individual supernova remnants) is that this emission is produced via shocks in the expanding superwind as it escapes the central starburst region. The hot high-velocity wind drives relatively fast ($v \geq 100$ km s^{-1}) shocks into the ambient ISM producing strong optical and infrared lines of low ionization. The starburst, in this scenario, would be unresolved in the near-infrared imaging data. The high-resolution 2 μm imaging of G90 suggests that both infrared nuclei are individually resolved, implying a significant fraction of the nuclear continuum may be produced in a starburst. A lower limit on the strength of the burst can be estimated as follows. The mechanical energy output from a constant star formation burst is typically $\leq 1\%$ of the bolometric radiant luminosity (Leitherer & Heckman 1995). In an instantaneous or exponentially declining burst, this can get up to a few percent of the radiant luminosity, but only for a short time period (when most of the massive stars are exploding as supernovae) after which it declines dramatically. Since a strong cooling line behind a radiative shock typically carries away ~1% of the available energy, we can estimate that the bolometric luminosity of the starburst responsible for the extended [Fe II] emission is $L_{\rm BOL} \geq 2 \times 10^{11}\ L_\odot$, if the burst provides all the energy required to power the [Fe II] emission. This lower limit is about 10% of the bolometric luminosity of Arp 220. A declining star formation rate burst seen at an age of $\geq 10^{7.5}$ yr would require a larger bolometric luminosity because the ratio of the mechanical energy input rate to the bolometric luminosity declines rapidly after this time. Similarly, if the efficiency of conversion to [Fe II] line luminosity is less than 1% the required bolometric luminosity will be larger than $2 \times 10^{11}\ L_\odot$.

Modelling the extended [Fe II] emission as arising from shocks associated with the expanding wind, implies that some fraction of the unresolved [Fe II] luminosity, $\sim 3 \times 10^{40}$ ergs s^{-1} in the 1.257 μm line, be directly associated with the starburst, presumably dominated by supernova remnants. Since this luminosity is $\sim \frac{1}{3}$ of the extended [Fe II] luminosity, the implied supernova rate is (~0.6 yr^{-1}). While lower than that derived by assuming all the extended [Fe II] is produced in supernova remnants, the implied bolometric luminosity of the burst ($\sim 6 \times 10^{11}\ L_\odot$) is still very large.

The bolometric luminosity of the starburst implied by the direct conversion of the nuclear [Fe II] luminosity to a supernova rate is not consistent with the ionizing luminosity derived from the Paβ luminosity, if both the [Fe II] and Paβ emission are produced in an ongoing starburst with a normal IMF slope (power-law index of 2.3–3.3) and large range of stellar masses (1–100 $M_\odot$). From the imaging data, the spatially unresolved Paβ luminosity is $\sim 4 \times 10^{40}$ ergs s^{-1} implying an ionizing photon rate of $\sim 6 \times 10^{53}$ s^{-1}, of a Lyman continuum luminosity of $\sim 1.2 \times 10^{43}$ ergs s^{-1} from the starburst. This is consistent with the upper limit on the ionizing photon rate of 7.5×10^{54} s^{-1} derived by Scoville et al. (1991) from the estimated thermal continuum flux at 2.7 mm. Ratios of the ionizing-to-bolometric luminosity as a function of time have been calculated by Leitherer & Heckman (1995) for a variety of starburst models. For IMF slopes between 2.35 (Salpeter-type) and 3.3 (solar neighborhood Miller-Scalo) and stellar masses between 1 and 100 $M_\odot$ the ratio of ionizing-to-bolometric luminosity ranges from 0.25 to 0.04 for constant star formation rates with ages between 10^7 and 10^8 yr. Taking the ionizing luminosity derived from the extended Paβ flux then implies a starburst bolometric luminosity in Arp 220 of $1.2\text{–}7.7 \times 10^{10}$ $L_\odot$, or only ~1%–5% of the bolometric luminosity of the galaxy. However, the nuclear [Fe II] emission implies a starburst bolometric luminosity of $\sim 6 \times 10^{11}\ L_\odot$, or a factor of nearly 10 larger than that implied by the ionizing flux. The same ionizing photon deficit exists in the nucleus of NGC 6240, where the strong [Fe II] emission (if powered by a starburst as suggested by van der Werf et al. 1993) implies a supernova rate of ~2 yr^{-1}, whereas the Bγ luminosity implies a very low flux of ionizing photons ($\sim 10^{54}$ s^{-1}).

The fact that Arp 220 appears to be deficient in the number of ionizing photons, compared to its infrared (taken as the bolometric) luminosity, has been noted previously by other authors (e.g., DePoy et al. 1987; Scoville et al. 1991) and used as an argument against star formation as the major source of power (see § 1). Here, we have shown that this is true even when deriving the starburst luminosity from the nuclear [Fe II] flux. Since the [Fe II] 1.257 μm and Paβ lines are close in wavelength, the effect of relative extinction are removed—underestimating the extinction increases not only the ionizing luminosity but the bolometric luminosity as well, through the larger [Fe II] and supernova rates, and thus does not remove the deficit.

There are three possible explanations for the deficit in the number of ionizing photons in the nucleus. First, a starburst with either a very low upper mass cutoff ($M < 20\ M_\odot$) or a sharply decreasing star formation rate could be responsible for the low ionizing photon rates. Both will reduce the number of the most massive stars. At about $t = 10^7\text{–}10^{7.5}$ yr after an instantaneous burst, the ionizing flux can be a factor of $10^{-2}\text{–}10^{-4}$ lower than the bolometric luminosity, and although the supernova rate is dropping rapidly as well, both can, for a short time, match what is seen in Arp 220 for a starburst having a total luminosity of a few times $10^{11}\text{–}10^{12}$ $L_\odot$ (Leitherer & Heckman 1995). Similar results have been found by Rieke et al. (1985) who fit a number of observations with an exponentially decreasing star formation rate burst having a very low upper mass cutoff of 31 $M_\odot$ and an age of 30–100 Myr. These authors concluded that up to 50% of the bolometric luminosity of Arp 220 could be generated by such a starburst.

Second, not all the ionizing photons generated in the nucleus may go into ionizing the surrounding gas. Dust in and around the nucleus may compete effectively for the ionizing photons from the most massive stars. As pointed out by Voit (1992), in regions of high column density, ≥90% of the ionizing luminosity can be directly thermalized by dust grains instead of being photoelectrically absorbed, causing a strong reduction in the number of ionizing photons counted by such means as measuring the free-free radio flux or the flux in a recombination line such as Paβ. This is often seen in Galactic H II-regions (Wood & Churchwell 1989). Similarly, the Paβ nebula may not be ionization bounded. The superwind and/or the

young stars in the starburst may create "holes" in the ISM through which ionizing photons can escape.

Third, much of the spatially unresolved [Fe II] emission may not be produced by supernova remnants in Arp 220. It could be photoionized by OB stars in a nuclear starburst, or by a buried (only along our line of sight) AGN. Since the strongest [Fe II] emission in starburst galaxies is associated with supernova remnants (Greenhouse et al. 1991; Forbes et al. 1993) it seems unlikely that supernova remnants would not play a major part in generating the [Fe II] emission in a luminous starburst in the nucleus of Arp 220. Also, the nuclear [Fe II] 1.257 μm-to-Paβ line flux ratio ($\sim$0.8) implies a nuclear [Fe II] 1.644 μm-to-Bγ line flux ratio of $\sim$2.1, much higher than that found for H II regions but comparable to that seen in some starburst galaxies where supernova remnants are known to mark local peaks in the [Fe II] emission (Greenhouse et al. 1991; Forbes et al. 1993). The alternative is that the majority of the spatially unresolved [Fe II] emission is excited by an AGN in the nucleus. If this [Fe II] emission exists in a narrow-line region surrounding an AGN in Arp 220, the ionizing photon deficit is removed. Although we cannot rule out the possibility that an AGN excites much of the spatially unresolved [Fe II] emission in Arp 220, it is unlikely that the AGN (if present) is also responsible for the extended [Fe II] emission (which dominates the total [Fe II] flux in Arp 220). This emission is present over large physical scales (2″–3″ corresponds to $\sim$750–1000 pc at the distance of Arp 220) and has a morphology different than that of Paβ. If an AGN dominates the ionization and heating of the extended gas, and the [Fe II] and Paβ both come from the NLR, they both should exhibit similar morphologies. This is clearly not the case in Arp 220.

If the majority of the [Fe II] emission in Arp 220 is produced in the expanding superwind, it should be shock excited and have a kinematic signature consistent with the outflowing gas mapped in the optical. We can measure neither of these properties with the current spectral data set. The importance of shock excitation could, in principle, be determined by measuring the temperature-sensitive [Fe II] 0.8617 μm/1.644 μm line flux ratio. Gas photoionized by a power-law continuum should have a higher temperature than gas excited via fast shocks, although the [Fe II] line ratio is also sensitive to density (Oliva et al. 1989; Graham et al. 1990b). High-resolution spectra of the near-infrared [Fe II] lines would allow a measurement of their profiles for comparison to the optical line-emitting gas involved in the outflow. The [Fe II] infrared and optical line ratios and line profiles should shed a great deal of light on the importance of the outflowing superwind in generating the strong extended [Fe II] emission we have mapped in Arp 220.

5. SUMMARY

A near-infrared imaging and spectroscopic study of Arp 220 in the J- and H-band atmospheric windows has revealed the following:

1. Arp 220 is a strong source of nuclear and circumnuclear [Fe II] and Paβ emission. Within the central 4″ the [Fe II] 1.257 μm line flux is 1.6×10^{-14} ergs cm^{-2} s^{-1}, and the Paβ line flux is 1.1×10^{-14} ergs cm^{-2} s^{-1}. An $A_V \sim 10$–12 mag is suggested both by measurement of the [Fe II] 1.257 and 1.644 μm lines and through comparison of these data to previously published optical emission-line images. We derive total [Fe II] 1.257 μm and Paβ luminosities of 13×10^{40} and 9.2×10^{40} ergs s^{-1}, respectively.

2. The [Fe II] and Paβ emission are both extended over the central 2″–3″, but with different morphologies. The Paβ line is strongly peaked at the position of the western K-band infrared nucleus, with a fainter "spur" in the direction of the eastern nucleus. The [Fe II] emission line shows a weak peak at the western nucleus along with diffuse emission extending to the east, but with no indication of a secondary maximum. The [Fe II] is more extended in the north-south direction than the Paβ line. Nearly 75% of the detected [Fe II] emission is spatially resolved.

3. The overall [Fe II]-to-Paβ line flux ratio in Arp 220 is consistent with that seen over similar spatial scales in Seyfert 2 galaxies, yet larger than what is measured in galaxies with nuclear starbursts. The morphological differences in the [Fe II] and Paβ emission-line maps lead to a spatially variable [Fe II]-to-Paβ line flux ratio in Arp 220. This line ratio is $\sim$0.8 at the position of the western nucleus and $\sim$2.0 at radii of up to 500 pc. The extended nature of the [Fe II] emission, the very different [Fe II] and Paβ morphologies, and the high off-nuclear [Fe II]-to-Paβ line flux ratios lead us to suggest that the extended [Fe II] emission is produced as a result of fast shocks at the base of the outflowing superwind which is responsible for the large-scale optical line-emitting nebula seen by Heckman et al. (1987). A starburst of more than $2 \times 10^{11}\ L_\odot$ is required to power the extended [Fe II] emission.

4. If the unresolved [Fe II] emission is produced by an ensemble of supernova remnants in the nucleus of Arp 220, the supernova rate ($\sim$0.6 yr^{-1}) is not consistent with the ionizing luminosity derived from the Paβ flux for a constant star formation rate burst having a normal IMF slope and a large range in stellar masses. This ionizing photon deficit could be explained by a starburst with a truncated IMF producing no stars above about 20 $M_\odot$, or by a decaying, instantaneous burst viewed about 10^7–10^8 yr after onset. Alternatively, dust in and around the Arp 220 nuclei could effectively compete for the ionizing photons produced in a luminous, but otherwise normal starburst, much of the ionizing radiation could escape through "holes" in the ISM, or an optically obscured AGN might excite much of the nuclear [Fe II] through photoionization in the NLR.

We would like to thank the night assistants at the Hale telescope, J. Carasco, S. Staples, and W. KcKinley, and the entire staff at the Palomar Observatory for their assistance in obtaining these data. Discussions with James Graham, Tim Heckman, and Matt Lehnert were most helpful, as were the suggestions of the referee. Infrared astronomy at Caltech is supported by grants from NASA and the NSF. This research has made use of the NASA/IPAC Extragalactic Database which is operated by the Jet Propulsion Laboratory, Caltech, under contract with NASA.

REFERENCES

Armus, L., Heckman, T. M., & Miley, G. K. 1989, ApJ, 347, 727
———. 1990, ApJ, 364, 471
Arp, H. C. 1966, Atlas of Peculiar Galaxies (Pasadena: California Institute of Technology)
Beck, S. C., & Beckwith, S. V. 1984, MNRAS, 207, 671
Blietz, M., Cameron, M., Drapatz, S., Genzel, R., Krabbe, A., van der Werf, P., Sternberg, A., & Ward, M. 1994, ApJ, 421, 92
Brocklehurst, M. 1971, MNRAS, 153, 471
Carico, D. P., Graham, J. R., Matthews, K., Wilson, T. D., Soifer, B. T., Neugebauer, G., & Sanders, D. B. 1990, ApJ, 349, L39

Condon, J. J. 1980, ApJ, 242, 894
DePoy, D. L., Becklin, E. E., & Geballe, T. R. 1987, ApJ, 316, L63
Elias, J. H., Frogel, J. A., Matthews, K., & Neugebauer, G. 1982, AJ, 87, 1029
Evans, I. N., Ford, H. C., Kinney, A. L., Antonucci, R. R. J., Amus, L., & Caganoff, S. 1991, ApJ, 369, L27
Forbes, D. A., & Ward, M. J. 1993, ApJ, 416, 150
Goodrich, R. W., Veilleux, S., & Hill, G. J. 1994, ApJ, 422, 521
Graham, J. R., Carico, D. P., Matthews, K., Neugebauer, G., Soifer, B. T., & Wilson, T. D. 1990a, ApJ, 354, L5 (G90)
Graham, J. R., Wright, G. S., & Longmore, A. J. 1987, ApJ, 313, 847
———. 1990b, ApJ, 352, 172
Greenhouse, M. A., Woodward, C. E., Thronson, H. A., Rudy, R. J., Rossano, G. S., Erwin, P., & Puetter, R. C. 1991, ApJ, 383, 164
Heckman, T. M., Amus, L., & Miley, G. K. 1987, AJ, 93, 276
———. 1990, ApJS, 74, 833
Kawara, K., Nishida, M., & Taniguchi, Y. 1988, ApJ, 328, L41
Leitherer, K., & Heckman, T. M. 1995, ApJS, 96, 38
Lester, D. F., Carr, J. S., Joy, M., & Gaffney, N. 1990, ApJ, 352, 544
Lester, D. F., Harvey, P. M., & Carr, J. S. 1988, ApJ, 329, 641
Lonsdale, C. J., Smith, H. E., & Lonsdale, C. J. 1993, ApJ, 405, L9
Lowe, R. P., Moorhead, J. M., & Wehlau, W. H. 1979, ApJ, 228, 191
Mazzarella, J. M., Soifer, B. T., Graham, J. R., Hefer, C. I., Neugebauer, G., & Matthews, K. 1992, AJ, 103, 413
Moorwood, A. F. M., & Oliva, E. 1988, A&A, 203, 278
Mouri, H., Kawara, K., & Taniguchi, Y. 1993, ApJ, 406, 52
Nussbaumer, H., & Storey, P. J. 1988, A&A, 193, 327
Norris, R. P. 1988, MNRAS, 230, 345
Oliva, E., & Moorwood, A. F. M. 1990, ApJ, 348, L5
Oliva, E., Moorwood, A. F. M., & Danziger, I. J. 1989, A&A, 214, 307
Osterbrock, D. E. 1989, Astrophysics of Gaseous Nebulae and Active Galactic Nuclei (Mill Valley: University Science Books)
Perez-Fournon, I., & Wilson, A. S. 1990, ApJ, 356, 456
Rieke, G. H., Cutri, R. M., Black, J. H., Kailey, W. F., McAlary, C. W., Lebofsky, M. J., & Elston, R. 1985, ApJ, 290, 116
Rieke, G. H., & Lebofsky, M. J. 1985, ApJ, 250, 87
Rieke, G. H., Lebofsky, M. J., Thompson, R. I., Low, F. J., & Tokunaga, A. T. 1980, ApJ, 238, 24
Robbins, R. R. 1968, ApJ, 151, 497
Sanders, D. B., Soifer, B. T., Elias, J., Madore, B., Matthews, K., Neugebauer, G., & Scoville, N. 1988, ApJ, 325, 74
Savage, B. D., & Mathis, J. D. 1979, ARA&A, 17, 73
Scoville, N. Z., Sargent, A. I., Sanders, D. B., & Soifer, B. T. 1991, ApJ, 366, L5
Shaya, E. J., Dowling, D. M., Currie, D. G., Faber, S. M., & Groth, E. J. 1994, AJ, 107, 1675
Smith, C. H., Aitken, D. K., & Roche, P. F. 1989, MNRAS, 241, 425
Soifer, B. T., Boehmer, L., Neugebauer, G., & Sanders, D. B. 1989, AJ, 98, 766
Sopp, H. M., & Alexander, P. 1991, MNRAS, 251, 112
van der Werf, P. P., Genzel, R., Krabbe, A., Blietz, M., Lutz, D., Drapatz, S., Ward, M. J., & Forbes, D. A. 1993, ApJ, 405, 522
Voit, G. M. 1992, ApJ, 399, 495
Waller, W. H., Kleinmann, S. G., & Ricker, G. R. 1988, AJ, 95, 1057
Ward, M. J., Geballe, T., Smith, M., Wade, R., & Williams, P. 1987, ApJ, 316, 138
Wilson, A. S., & Ulvestad, J. S. 1983, ApJ, 275, 8
Wood, D. O. S., & Churchwell, E. 1989, ApJS, 69, 831